Chemical Engineering Journal 282 (2015) 20–28

Contents lists available at ScienceDirect

Chemical Engineering Journal

journal homepage: www.elsevier.com/locate/cej

Temperature-Scanning Method for the kinetic studies of CO oxidation over ceria–zirconia supported gold catalysts

Miguel-Ángel Gómez-García [a], Noel A. Gómez Mendoza [a], Izabela Dobrosz-Gómez [b,*], Edison GilPavas [c], Jacek Rynkowski [d]

[a] Grupo de Investigación en Procesos Reactivos Intensificados con Separación y Materiales Avanzados (PRISMA), Departamento de Ingeniería Química, Facultad de Ingeniería y Arquitectura, Universidad Nacional de Colombia – Sede Manizales, Cra 27 64-60, Apartado Aéreo 127, Manizales, Colombia
[b] Grupo de Investigación en Procesos Reactivos Intensificados con Separación y Materiales Avanzados (PRISMA), Departamento de Física y Química, Facultad de Ciencias Exactas y Naturales, Universidad Nacional de Colombia – Sede Manizales, Cra 27 64-60, Apartado Aéreo 127, Manizales, Colombia
[c] GIPAB: Grupo de Investigación en Procesos Ambientales, Departamento de Ingeniería de Procesos, Universidad EAFIT, Cra 49 7sur50, Medellín, Colombia
[d] Institute of General and Ecological Chemistry, Lodz University of Technology, 90-924 Lodz, Zeromskiego 116, Poland

HIGHLIGHTS

- Variation of Temperature Scanning Method let to optimize catalyst composition.
- Extended reaction surface plot identifies Au/$Ce_{0.75}Zr_{0.25}O_2$ catalyst as optimal one.
- For all catalysts activation energy and pre-exponential factors were determined.
- Support redox properties controlled the performance of the Au/$Ce_{1-x}Zr_xO_2$ catalysts.
- Fitted MvK model predicted superficial reaction and catalyst surface re-oxidation.

GRAPHICAL ABSTRACT

Predicted surface plot of conversion – temperature – catalyst composition (2 wt.% Au/$Ce_{1-x}Zr_xO_2$ washed with ammonia) as a tool for catalyst optimization (dots represent experimental data).

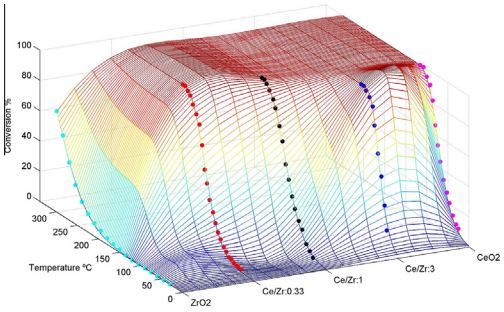

ARTICLE INFO

Article history:
Available online 14 March 2015

Keywords:
Kinetic studies
Temperature-Scanning Method
Gold catalyst
Ceria–zirconia mixed oxide
CO oxidation
Catalyst composition optimization

ABSTRACT

The experimental data of CO oxidation over the series of 2 wt.% Au/$Ce_{1-x}Zr_xO_2$ ($x = 0, 0.25, 0.5, 0.75, 1$) catalyst were analyzed using a variation of the Temperature Scanning Method with the aim of catalyst's composition optimization. The catalysts were prepared by the Direct Anionic Exchange technique. The kinetic of CO oxidation was quantified by conversion–rate–temperature (X, r, T) triplets, calculated from raw data obtained using a plug flow reactor, working at oxygen stoichiometric, rich, and lean conditions. The data were fitted to the Mars-van Krevelen adsorption-reaction model (MvK). The results showed that the MvK model is able to predict the superficial reaction and the re-oxidation of the catalyst surface. Additionally, the data at oxygen lean conditions revealed the distinctive characteristic of Ce-containing catalysts, which act as oxygen buffer by releasing-uptaking oxygen. The obtained values of the fitted parameters allowed re-mapping raw data onto the conversion–temperature–catalyst composition surface plot and their application as a tool for the optimization of catalyst composition.

* Corresponding author.
E-mail address: idobrosz-gomez@unal.edu.co (I. Dobrosz-Gómez).

http://dx.doi.org/10.1016/j.cej.2015.03.015
1385-8947/

1. Introduction

Catalytic oxidation of CO has received extensive attention due to its significance in practical applications, particularly in the context of breathing air purification in the closed spaces and reduction of cold start automotive exhaust emissions. This reaction, developed on platinum group based catalysts, has been studied and extensively reviewed [1] since the classic work of Langmuir [2]. Afterwards, several research groups have also demonstrated high efficiency of gold nanoparticles supported on partly reducible oxides in CO oxidation [3–7].

For this reaction, several kinetic rate models have been proposed in the open literature [1,8]. They are based on two widely accepted possible reaction mechanisms: Langmuir–Hinshelwood (LH) and Mars van Krevelen (MvK) [5]. The LH reaction model (i) includes the following set of steps: (i.1) competitive adsorption of CO and oxygen molecules from the gas phase on catalyst surface, (i.2) oxygen dissociation, (i.3) reaction between the adsorbed molecules/atoms, and finally (i.4) desorption of CO_2 to the gas phase. On the other hand, the MvK mechanism (ii) consists of: (ii.1) the metal/support oxidation in a separate and independent steps, (ii.2) adsorption of CO from the gas phase on the oxide, (ii.3) reaction between the adsorbed CO and catalyst surface oxygen, accompanied with the creation of oxygen vacancies, (ii.4) CO_2 desorption from the catalyst surface, and (ii.5) fast and irreversible refilling of the resulting oxygen vacancies by oxygen from the gas phase, in separate step (as in ii.1). As a consequence, LH and MvK models can be described by different kinetic rate expressions. One of the most important differences could be the fact that LH model presents a controversial tendency to predict low CO oxidation rates at high temperatures [8–12], as it could be seen for a set of experimental data obtained in this work (Appendix 1). Consequently, the reversibility of CO oxidation at these reaction conditions can be expected; statement that has not been confirmed experimentally using noble metal based catalysts. Moreover, the other authors [9] have already claimed that the permanence of oxygen radicals' on catalyst surface and their constant availability for the reaction are inconsistent with restrictions of LH model. Therefore, in this work, the MvK model was selected to fit the experimental data.

Many researchers have tried to perform temperature-programmed runs and to "deduce the kinetics" observing the light-off point during the temperature ramping program. Thus, Wojciechowski and Rice [9] developed the Temperature Scanning Method (TSM), at which experiments consist of operating the reactor over a period of time, varying the temperature in a programmed way. During each run, the temperature and conversion data are registered at the outlet of the reactor. Subsequently, the reaction rate can be calculated basing on the obtained raw data by splining the discrete conversion (X) – residence time (τ) data (at a constant temperature) and evaluating the $dX/d\tau$ to yield the rates, r, at these conditions (τ, X, T) [9]. Next, the (X, r, T) triplets can be used for rate law parameters fitting. Consequently, surface plots, usually, tridimensional correlation between residence time, temperature and conversion can be obtained. Finally, the catalyst performance can be predicted.

Thus, the goal of this work was to develop a numerical technique to analyze the reaction kinetics of CO oxidation using a variation of the TSM (including the catalyst composition as a variable for optimization). In fact, we show how to win more insight into the chemical reaction kinetics by extending the original methodology of Wojciechowski and Rice [8,9]. As far as we know, no similar analysis has been reported in the open literature. Thus, the kinetic of CO oxidation was quantified by conversion–rate–temperature (X, r, T) triplets obtained for a series of 2 wt.% $Au/Ce_{1-x}Zr_xO_2$ (x = 0, 0.25, 0.5, 0.75, 1) catalysts and their corresponding supports. Finally, the obtained kinetic results were discussed based on morphological, structural and redox (using CO-TPR) properties of the studied catalysts.

2. Experimental

2.1. Catalyst synthesis

A series of $Ce_{1-x}Zr_xO_2$ (x = 0.25, 0.5, 0.75) solid solutions, characterized with different Ce/Zr molar ratio (Ce/Zr = 3, 1, 0.33, respectively), CeO_2 and ZrO_2, used as support for Au, were prepared by the sol–gel like method, based on a thermal decomposition of mixed propionates [13]. The starting materials, zirconium (IV) acetylacetonate [$Zr(CH_3COCH_2COCH_3)_4$, Avocado, purity 99.9%] and/or cerium (III) acetylacetonate hydrate [$Ce(CH_3COCH_2COCH_3)_3{\cdot}H_2O$, Sigma–Aldrich, purity 99.9%] were dissolved in boiling propionic acid in concentration of 0.12 M. Next, boiling solutions were mixed and the solvent was evaporated until a resin was obtained. All samples were calcined in air at 550 °C for four hours. Hydrogen tetrachloroaurate (III) trihydrate [$HAuCl_4{\cdot}3H_2O$, Sigma–Aldrich, purity 99.9%] was used as a gold precursor. The supported Au catalysts were prepared by the Direct Anionic Exchange (DAE) method of gold species with hydroxyl groups of the support [14,15]. The optimization of catalyst's synthesis conditions was in details presented previously [16]. In order to remove the residual chlorine from the catalysts, responsible for Au agglomeration during thermal treatment, an ammonia washing procedure prior to the drying process was applied, as described previously [10,11].

2.2. Catalyst characterization

Nitrogen adsorption/desorption isotherms at −196 °C were measured using Sorptomatic 1900 apparatus (Carlo-Erba). Prior to the measurement, all samples were degassed for 4 h at 250 °C. The specific surface area, S_{BET}, was calculated using BET equation [10,11].

Atomic Absorption Spectroscopy (AAS) analyses were performed with a Solaar M6 Unicam spectrophotometer in order to estimate the amount of Au deposited on supports, as described previously [11].

High Resolution Transmission Electron Microscopy (HRTEM) measurements were carried out using high resolution microscope EM-002B (TOPCON), at an acceleration voltage 200 kV, equipped with energy dispersive spectrometer (EDS). To determine an average Au particle size and to define their distribution more accurate, at least 500 particles of each catalyst were chosen for analysis. Moreover, many different HRTEM images of each catalyst sample have been analyzed, in details described previously [11].

Temperature Programmed Reduction (TPR-CO) experiments were carried out by PEAK-4 apparatus [17], using CO as reducing agent. The apparatus was equipped with an infrared gas analyser (Fuji Electric Systems Co., type: ZRJ-4) to follow CO_2 formation. TPR-CO experiments were performed using a CO/He (5 vol.% CO, 95 vol.% He) gas mixture, with a flow rate of 40 $cm^3\ min^{-1}$, in the temperature range of 25–850 °C, with a ramp rate of 15 °C min^{-1}. Powdered samples of 100 mg were exposed to dry Ar at 250 °C for 1 h before the reduction.

2.3. Reactor set-up

CO oxidation reaction was carried out at atmospheric pressure in a quartz flow microreactor containing 100 mg of sample in a

fixed bed. Using a series of mass flow controllers, three different gas mixtures containing 1.6 vol.% CO and 3.3 vol.% O_2 (oxygen rich); 3.4 vol.% CO and 1.7 vol.% O_2 (oxygen stoichiometric) and 4.1 vol.% CO and 1.0 vol.% O_2 (oxygen lean) and He as eluent gas were used. Experiments were performed in the temperature range of either 25–550 °C (supports) or 25–300 °C (gold catalysts), with a ramp rate of 5 °C min^{-1}, and a flow rate of 50 cm^3 min^{-1}. The catalytic experiments were repeated several times in order to verify their reproducibility. Gas chromatograph fitted with molecular sieves 5 Å, equipped with a thermal conductivity detector was used to perform the analysis of both CO and O_2 concentration. The CO conversion was calculated as follows:

$$\%\ \text{CO conversion} = \frac{[CO]_{in} - [CO]_{out}}{[CO]_{in}} \times 100 \quad (1)$$

where $[CO]_{in}$ and $[CO]_{out}$ are the inlet and outlet concentrations of CO, respectively.

3. Kinetic parameters assessment

The MvK rate expression was used to fit the data obtained in the present study. This model can be presented as follows [18]:

$$-r_{CO} = \frac{k_1 k_2 P_{CO} P_{O_2}}{k_1 P_{CO} + k_2 P_{O_2}} \quad (2)$$

where P_{CO} and P_{O_2} are the partial pressures of carbon monoxide and oxygen, respectively. The temperature dependency of the rate constants (k_i) was correlated by an Arrhenius type equation with k_{io}: pre-exponential factor and (E_a/R): activation energy [K], as follows:

$$Ln(k_i) = Ln(k_{oi}) - \frac{E_{ai}}{RT} \quad (3)$$

Since the experimental devise corresponds to an isothermal packed bed reactor (PBR), a differential molar-flow balance, in the terms of catalyst weight, can be proposed as follows:

$$\frac{dF_i}{dw} = r_i \quad (4)$$

Fitting procedure consisted of solving Eq. (4) which depends on the kinetic parameters included in Eqs. (2) and (3). Eq. (4) was numerically solved using a Runge–Kutta integration method [19]. Thus, since available experimental data were conversion vs. temperature (only the light-off curve's ascending part points of the data set were taken into account), a k value was guessed to start calculations for each temperature. If CO conversion at the end of the reactor corresponded to the experimental one (v. g., the error is within a tolerance), k can be accepted as the solution for that temperature; if it was not, a new k value was recalculated by a Newton–Raphson method [19] and the fitting procedure started again. In this way, r_{CO} can be presented as a function of four variables (k_{o1}, E_{a1}, k_{o2}, E_{a2}). If we denote by $r(P_{CO}, P_{O_2}$ the rate values obtained experimentally, to fit correctly the data, it will be necessary to find the x parameters that minimize the sum of squares, which correspond to the Arrhenius type constants in Eq. (3), as shown in Eq. (5):

$$f(x) = \sum_{P_{CO}, P_{O_2}} \left[r_{CO}(x, P_{CO}, P_{O_2}) - r_{CO}(P_{CO}, P_{O_2}) \right]^2 \quad (5)$$

4. Results

4.1. Catalyst characterization results

Table 1 presents specific surface area (S_{BET}), real Au loading, average Au particle size and summary of TPR-CO results for $Ce_{1-x}Zr_xO_2$ supports and 2 wt.% $Au/Ce_{1-x}Zr_xO_2$ catalysts. CeO_2 was characterized with the highest S_{BET} and ZrO_2 with the lowest one. In the case of Ce–Zr binary oxides, the substitution of Ce by an increasing amount of Zr decreased their surface area. The $Au/Ce_{1-x}Zr_xO_2$ catalysts presented similar S_{BET} to their corresponding oxide supports. Their real Au loading was lower than the nominal one due to the loss of Au in the ammonia washing step during catalyst preparation, in details described in [10,11]. The majority of the Au particles (mainly spherical) supported on $Ce_{1-x}Zr_xO_2$ were in the range of 1–7 nm, with an average size as shown in Table 1 [10,11].

Previously, we also discussed in details the reducibility process (TPR-CO) of both $Ce_{1-x}Zr_xO_2$ [10] and 2 wt.% $Au/Ce_{1-x}Zr_xO_2$ [11]

Table 1
Summary of relevant properties of $Ce_{1-x}Zr_xO_2$ and 2 wt.% $Au/Ce_{1-x}Zr_xO_2$ catalysts.

Oxide supports/catalyst denotation (Au wt.% content corresponds to the nominal)	Real Au loading[a] (wt.%)	Specific surface area (S_{BET})[b] (m^2 g^{-1})	Average Au particle size[c] (nm)	TPR-CO results[d]			
				T_0	T_1	T_2	T_3
CeO_2	–	58.1	–	270	430	–	840
$Ce_{0.75}Zr_{0.25}O_2$	–	50.1	–	260	460	–	760
$Ce_{0.5}Zr_{0.5}O_2$	–	46.5	–	280	500	–	760
$Ce_{0.25}Zr_{0.75}O_2$	–	41.0	–	300	530	–	–
ZrO_2	–	4.5	–	700	850	–	–
2 wt.% Au/CeO_2	1.79	51.5	4.0	110	150	330	840
2 wt.% $Au/Ce_{0.75}Zr_{0.25}O_2$	1.68	49.5	3.9	85	260	380	740
2 wt.% $Au/Ce_{0.5}Zr_{0.5}O_2$	1.74	45.0	4.0	135	270	400	720
2 wt.% $Au/Ce_{0.25}Zr_{0.75}O_2$	1.71	40.7	4.1	140	380	–	–
2 wt.% Au/ZrO_2	1.45	3.8	5.6	670	820	–	–

Determined by:
[a] AAS.
[b] BET.
[c] HRTEM (details in Appendix 2a).
[d] TPR-CO (T_0: the initial reduction temperature; T_1: the reduction temperature of the most easily reducible surface capping oxygen, the maximum corresponding to the low temperature reduction peak; T_2: the reduction temperature of support intermediate phases (surface or subsurface Ce^{4+}) as the origin of the low temperature reduction peak; T_3: the temperature of bulk reduction, the maximum corresponding to the high temperature reduction peak), in details in Appendix 2b.

catalysts. Summarizing, reduction of CeO_2 by CO occurs in two stages with the maxima at 430 °C and 840 °C. They can be ascribed to the reduction of the most easily reducible surface capping oxygen and bulk reduction, respectively. ZrO_2 shows the highest resistance to the reduction (Table 1). The reducibility of Ce/Zr mixed oxides depends on its molar ratio. One can see the slight shift in the maximum of the low-temperature peak (T_1) towards higher temperature, with a decrease in Ce/Zr molar ratio (Table 1). It can be related to the shorting or lengthening of metal–oxygen bonds due to the phase distortion, changing the barrier of energy for the oxygen migration in the bulk. In the presence of well dispersed Au nanoparticles, Ce^{4+}, surface and subsurface one, located at different chemical environments of support, becomes more susceptible to the reduction at much lower temperatures (Table 1). On the other hand, their reducibility at a high temperature remains almost unchanged.

4.2. CO oxidation reactivity test

4.2.1. Oxygen stoichiometric and rich conditions

The symbols in Figs. 1 and 2 represent the raw conversion–reactor outlet temperature data for oxygen stoichiometric and rich conditions, respectively. They include information for supports (Figs. 1a and 2a) and 2 wt.% $Au/Ce_{1-x}Zr_xO_2$ catalysts (Figs. 1b and 2b).

After comparing the catalytic behavior shown in Fig. 2, in general, it is possible to say CO conversion is shifted to lower temperatures at oxygen rich conditions. This could be a consequence of fast and irreversible refilling of the resulting catalyst oxygen vacancies by oxygen from the gas phase. Such effect is more evident for ZrO_2 based catalyst, basically due to its poor bulk oxygen mobility which is highly improved by the presence of gold particles.

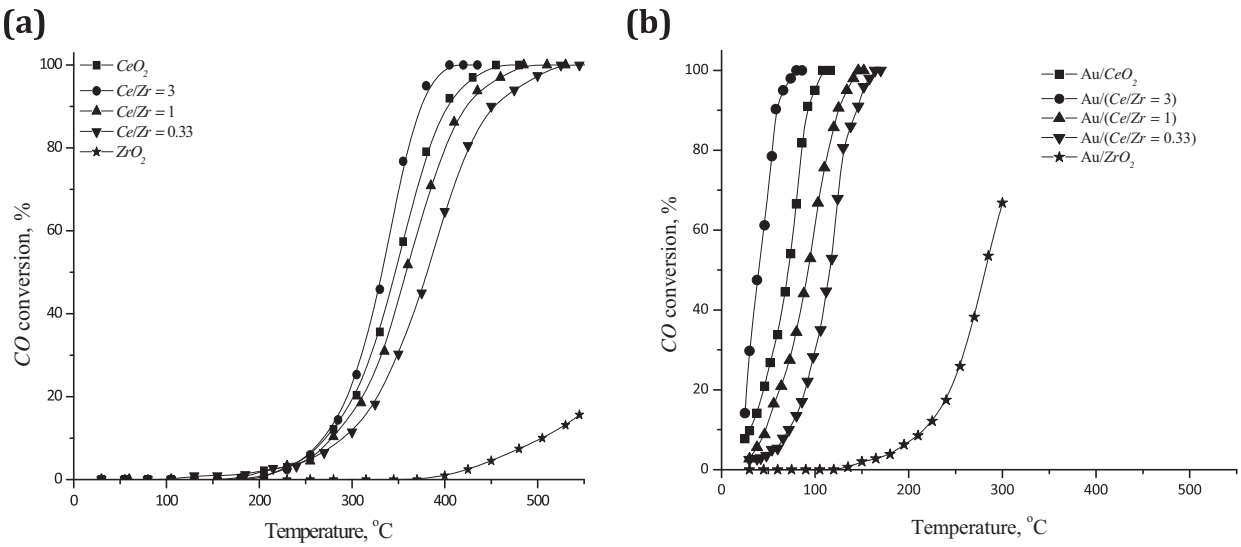

Fig. 1. Experimental data of CO oxidation at stoichiometric conditions (symbols) and fitted curves using MvK model (lines) for: (a) oxide supports and (b) 2 wt.% $Au/Ce_{1-x}Zr_xO_2$ catalysts.

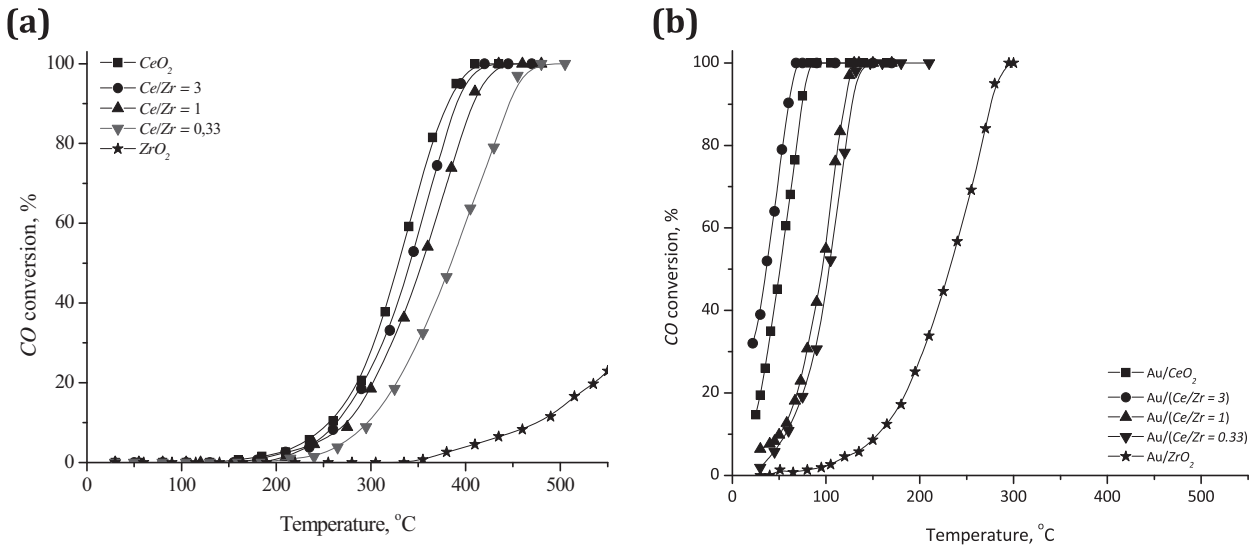

Fig. 2. Experimental data of CO oxidation at oxygen rich conditions (symbols) and fitted curves using MvK model (lines) for: (a) oxide supports; and (b) 2 wt.% $Au/Ce_{1-x}Zr_xO_2$ catalysts.

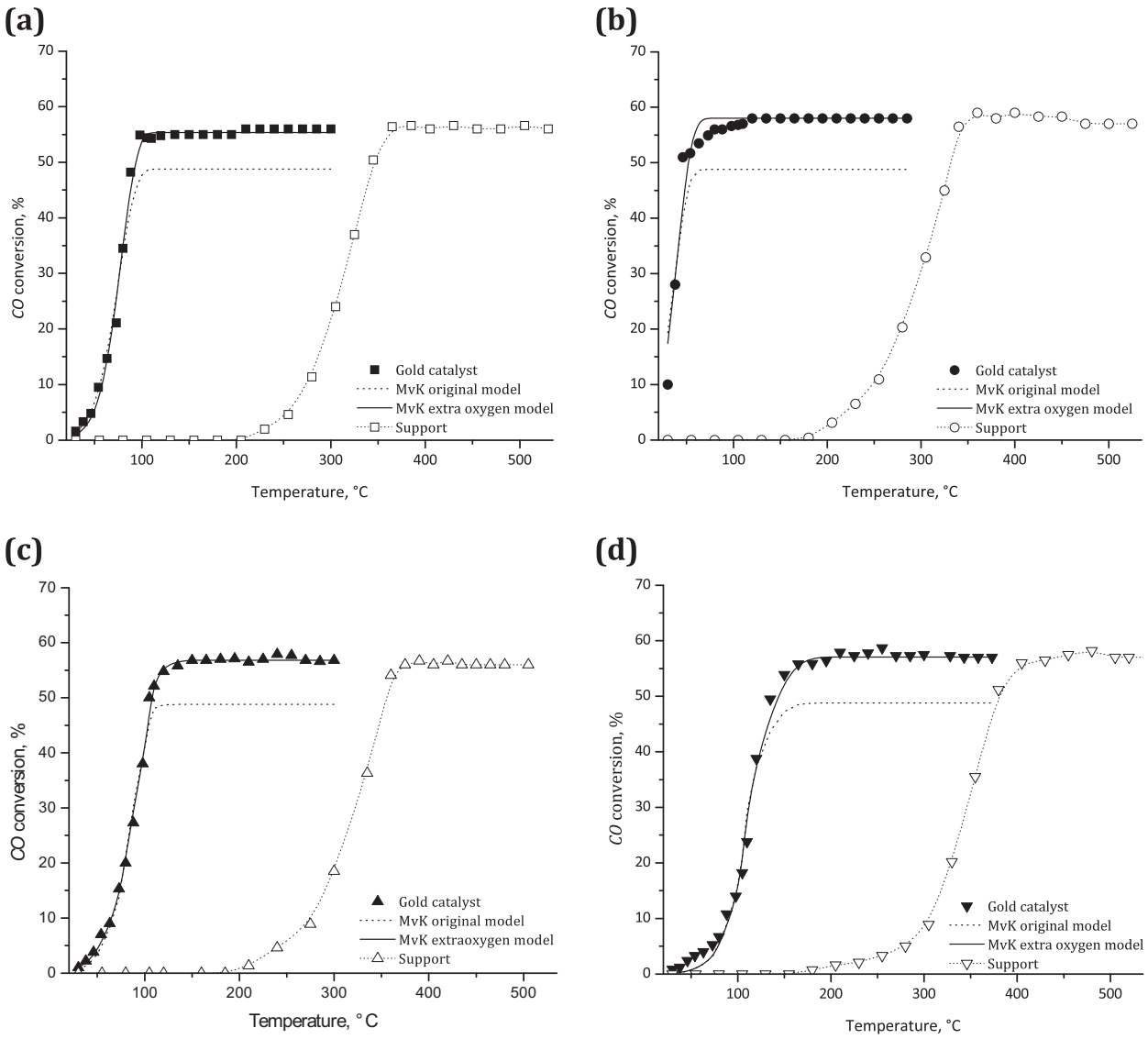

Fig. 3. Experimental data of CO oxidation at lean conditions and fitted curves for several 2 wt.% Au/$Ce_{1-x}Zr_xO_2$ catalysts: (a) Au/CeO_2; (b) Au/(Ce/Zr = 3); (c) Au/(Ce/Zr = 1); and (d) Au/(Ce/Zr = 0.33).

The smooth light-off behavior is observed and CO conversion increases with the increase in the reaction temperature. At temperatures below 200 °C, for all $Ce_{1-x}Zr_xO_2$ oxides, neither CO conversion nor reduction by CO was observed. Both their activity and reducibility increases at temperature above 250 °C. At higher temperatures of reaction, their catalytic performance depends on Ce/Zr molar ratio, with maximum obtained for $Ce_{0.75}Zr_{0.25}O_2$ (Ce/Zr molar ratio = 3). The similar catalytic performance of $Ce_{0.75}Zr_{0.25}O_2$ and CeO_2 suggests that cerium is responsible for the activity of mixed oxides in CO oxidation under studied conditions. The activity of ZrO_2, in the studied temperature range, was the lowest one (25% CO conversion at 550 °C) due to its significantly lower reducibility (Table 1). In the presence of well dispersed Au nanoparticles, the following order of activity, at significantly lower temperature, was observed: Au/$Ce_{0.75}Zr_{0.25}O_2$ > Au/CeO_2 > Au/$Ce_{0.5}Zr_{0.5}O_2$ > Au/$Ce_{0.25}Zr_{0.75}O_2$ > Au/ZrO_2. One can see that the sequence of increasing activity follows the sequence of increasing reducibility of catalysts. It indicates the

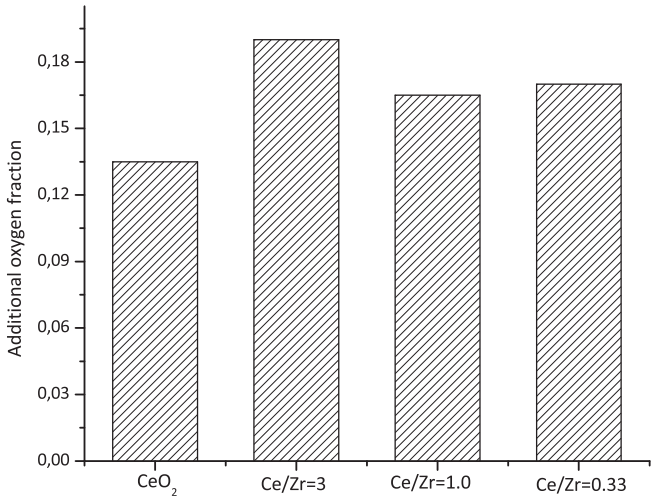

Fig. 4. Additional oxygen fraction needed to fix experimental data at oxygen lean conditions, for different 2 wt.% Au/$Ce_{1-x}Zr_xO_2$ catalyst compositions.

importance of the support redox properties in the creation of the catalytic performance of Au/$Ce_{1-x}Zr_xO_2$. In fact, for Au/CeO_2 catalyst the CO adsorption was previously observed on both CeO_2 (Ce^{4+}–CO) and Au^{3+}, Au^{+}, Au^{0} species [20]. Therefore, the synergetic effect between the support and Au nanoparticles at the interface can be claimed.

4.2.2. Oxygen lean conditions

The symbols in Fig. 3 represent the raw conversion–reactor outlet temperature data for oxygen lean conditions, obtained on $Ce_{1-x}Zr_xO_2$ and Au catalyst (2 wt.% Au/$Ce_{1-x}Zr_xO_2$). As it could be seen, the presence of Au effectively promotes the CO oxidation at low temperatures. The promoting effect of Au nanoparticles on the reducibility of different metal-oxide supports has already been observed [21–23]. Such behavior could be related to the adsorption of CO molecules on well dispersed metallic Au particles and next to the migration by a spillover process from the Au particles on the support surface. This process could be favored by a high dispersion of gold on the support surface. Additionally, it has been claimed that the presence of gold causes a decrease in the strength of the surface Ce–O bonds adjacent to gold atoms, leading to higher surface lattice oxygen mobility, as proposed by Scirè et al. [24]. These findings indicate the role of a support in creation of the catalytic performance of supported Au nanoparticles in CO oxidation.

4.3. Data fitting results

The raw conversion-reactor outlet temperature data presented in Figs. 1–3 can be used for conversion–rate–temperature

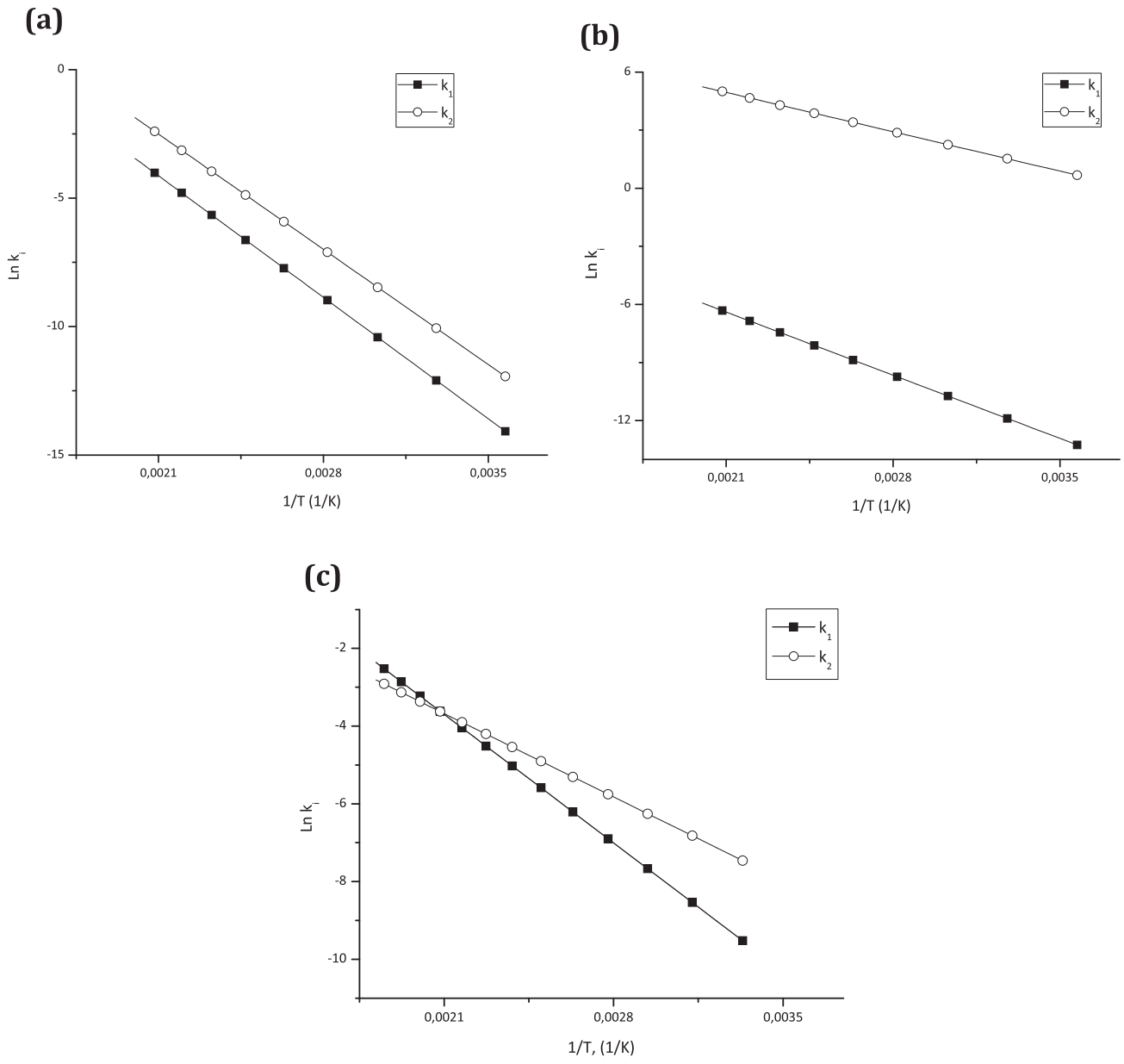

Fig. 5. Experimental data of CO oxidation and curves of fitting results for different oxygen conditions: (a) stoichiometric; (b) rich and (c) lean.

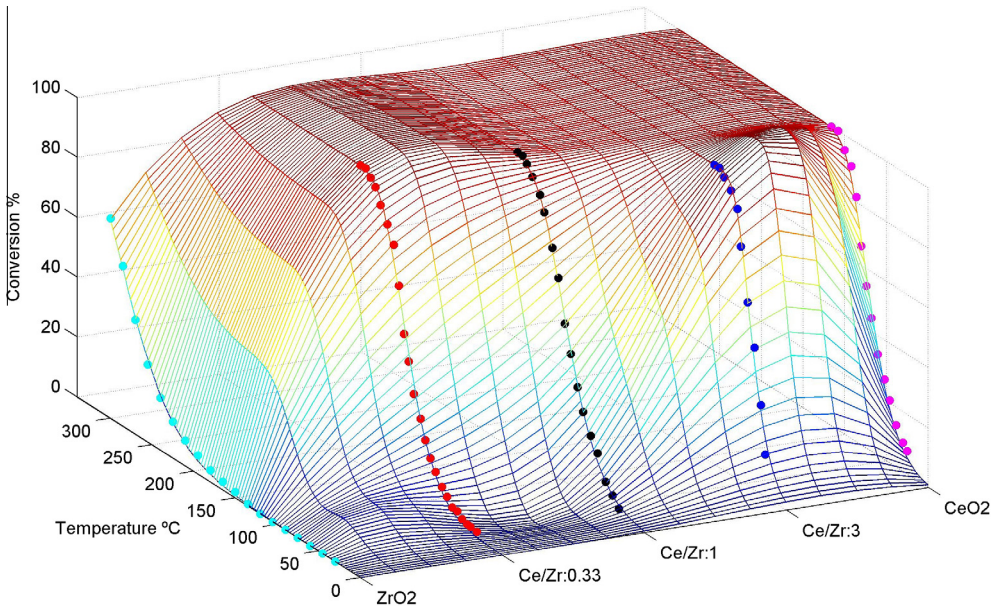

Fig. 6. Predicted surface plot of conversion–temperature–catalyst composition (2 wt.% $Au/Ce_{1-x}Zr_xO_2$) as a function of Ce/Zr molar ratio. Dots represent experimental data.

(*X*, *r*, *T*) triplets preparation. These figures also include the correlated curves obtained using proposed fitting method. The adjusted MvK model is able to predict experimental data at stoichiometric and rich conditions, even if some of them present a very fast increase in conversion with reaction temperature. For all studied catalysts, the curves correlated using MvK model present the increase in CO conversion with an increase in reaction temperature, reaching a maximum and constant value. Their further extrapolations to temperatures higher than the experimental ones do not predict any decrease in both the reaction rate and CO conversion (Appendix 1). Therefore, as explained above, the MvK model can be suggested as more relevant, instead of LH one, to describe kinetics of CO oxidation over $Ce_{1-x}Zr_xO_2$ and $Au/Ce_{1-x}Zr_xO_2$ catalysts. Consequently, the principal role of Au in CO oxidation over $Au/Ce_{1-x}Zr_xO_2$ catalysts can be related to the promotion in transformation process of reversibly adsorbed or inactive surface oxygen into irreversibly adsorbed species, active in CO oxidation, as previously proposed by Morgan et al. [5]. However, special attention deserves the fitting results obtained at lean conditions (Fig. 3). The original MvK model was not able to predict the experimental conversion data. In fact, the maximum CO conversion which can be obtained at lean conditions is ca. 50%. On the other hand, according to the TPR-CO results, Table 1, the highest quantity of oxygen that can be involved in the reaction is available at the same temperatures at which CO oxidation occurs. It suggests that the reaction involves both gas phase oxygen and surface – bulk oxygen, indicating the ability of Ce-containing oxides to supply reactive oxygen to Au active species for CO oxidation. It supports the idea of Ce acting as an oxygen buffer by releasing-uptaking oxygen through the redox processes involving Ce^{4+}/Ce^{3+} redox couple [25–27]. Moreover, considering TPR-CO experiments as reaction tests performed under totally anaerobic conditions (without oxygen present in the gas phase), the activity seems to be dependent on the ability of the oxide to release first the surface and then bulk oxygen. Considering that extra-oxygen is available from catalyst's surface-bulk, it was possible to fit and to predict the catalyst behavior (Fig. 3). The quantity of additional oxygen fraction required for data fitting is presented in Fig. 4, for different catalyst compositions. It was assessed from fitting experimental data and mass balances constrains. As expected, the most active catalyst (2 wt.% Au/(Ce/Zr = 3)) presents the highest oxygen mobility.

Fig. 5 presents the values of kinetics parameters for 2 wt.% $Au/Ce_{1-x}Zr_xO_2$ catalyst (with Ce/Zr molar ratio equals to 3), estimated for the MvK model using the proposed fitting procedure. This Arrhenius plot shows how activation energy and temperature affect the sensitivity of the reaction rate. As expected, marked differences in k_i values can be recognized between experiments performed at different conditions (oxygen content). Therefore, some additional observations can be pointed out. At oxygen stoichiometric conditions (Fig. 5a) k_i lines show the steeper slope. Therefore, they are characterized with higher activation energy than that at oxygen lean conditions (lines in Fig. 5c suggest lower activation energy, flatter slope). It means that in the same temperature range, the reaction with higher activation energy changes more rapidly than that with lower one.

The fitted parameters allow re-mapping raw data onto the conversion-temperature-catalyst composition surface plot. The example of such surface plot is presented in Fig. 6. Basing on the predicted surface it is possible to read off any point within all area including the experimental data and to sieve out the best conditions for the analyzed variables. Thus, the optimal CO oxidation conditions could be foreseen for the studied variables. In this case, they correspond to the catalyst with a composition very close to 2 wt.% $Au/Ce_{0.75}Zr_{0.25}O_2$.

5. Conclusions

A variation of the Temperature Scanning Method (TSM) was applied to analyze the experimental data of CO oxidation over the series of 2 wt.% $Au/Ce_{1-x}Zr_xO_2$ ($x = 0$, 0.25, 0.5, 0.75, 1) catalysts, with the aim of catalyst's composition optimization. The sequence of increasing activity followed the progression of

increasing catalysts reducibility, indicating the importance of support redox properties in controlling the performance of the $Au/Ce_{1-x}Zr_xO_2$ catalysts. The kinetic of CO oxidation was quantified by conversion–rate–temperature (X, r, T) triplets and the obtained data were fitted to the MvK adsorption-reaction model. For all studied catalysts, the activation energy and pre-exponential factors were determined. The obtained parameters allow defining an extended reaction surface, when plotted on the composition plane. It let clearly to identify the optimal catalyst composition (2 wt.% $Au/Ce_{0.75}Zr_{0.25}O_2$). The MvK model was suggested as more relevant, instead of L-H one, to describe kinetics of CO oxidation over $Ce_{1-x}Zr_xO_2$ and $Au/Ce_{1-x}Zr_xO_2$ catalysts. Consequently, the principal role of Au in CO oxidation over $Au/Ce_{1-x}Zr_xO_2$ catalysts can be related to the promotion in transformation process of reversibly adsorbed or inactive surface oxygen into irreversibly adsorbed species active in CO oxidation. Additionally, at oxygen lean conditions, the activity seems to be dependent on the ability of the oxide to release first the surface and then bulk oxygen. Thus, considering that extra-oxygen is available from catalyst's surface-bulk, it was possible to fit properly the observed catalyst activity. Finally, the proposed fitting procedure, based on MvK expression, can be considered as successful for all conditions tested for CO oxidation reaction.

Acknowledgements

Universidad Nacional de Colombia, Sede Manizales and DIMA (Dirección de Investigaciones de la Universidad Nacional de Colombia, Sede Manizales) are gratefully acknowledged.

Appendix 1

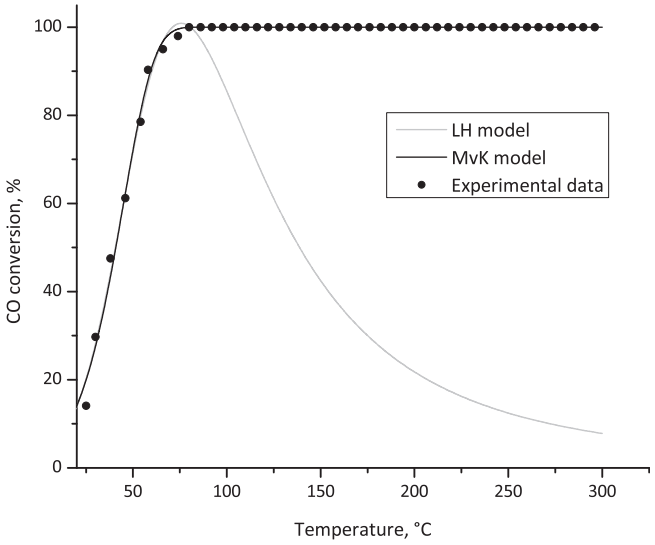

Prediction of MvK and LH models at extrapolated temperatures (dots represent experimental data of CO oxidation over 2 wt.% $Au/Ce_{0.75}Zr_{0.25}O_2$ catalyst washed with ammonia).

Appendix 2. Catalysts characterization

a. HRTEM images and Au particle size distribution of studied 2 wt.%$Au/Ce_{1-x}Zr_xO_2$ catalysts

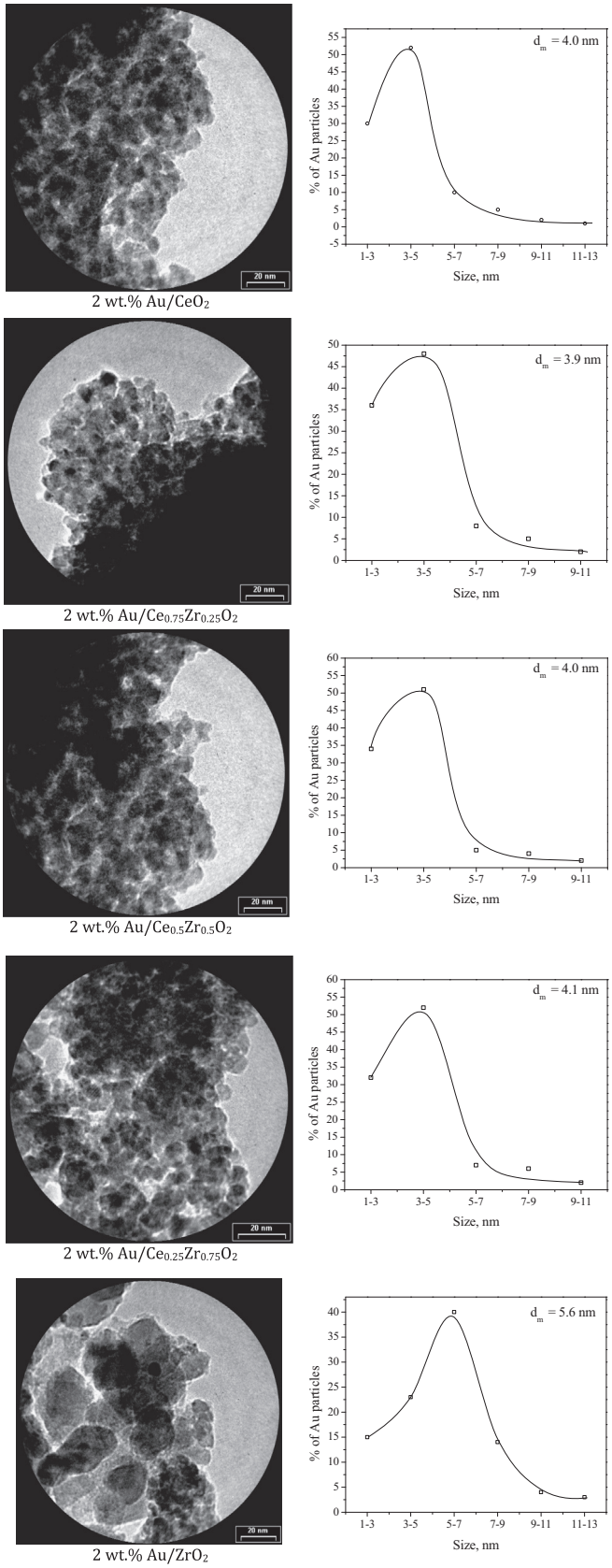

b. TPR-CO profiles of studied oxide supports and 2 wt.%Au/$Ce_{1-x}Zr_xO_2$ catalysts (based on [11])

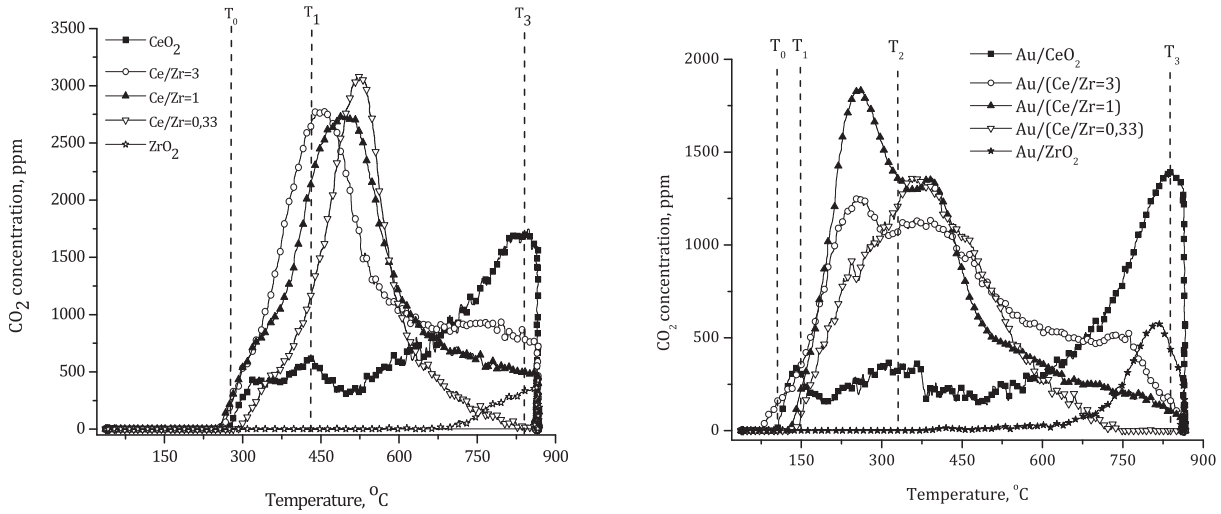

References

[1] S. Royer, D. Duprez, ChemCatChem 3 (2011) 24.
[2] I. Langmuir, Trans. Faraday Soc. 17 (1922) 621.
[3] M. Haruta, T. Kobayashi, H. Sano, N. Yamada, Chem. Lett. 2 (1987) 405.
[4] J. Saavedra, C. Powell, B. Panthi, C.J. Pursell, B.D. Chandler, J. Catal. 307 (2013) 37.
[5] K. Morgan, K.J. Cole, A. Goguet, C. Hardacre, G.J. Hutchings, N. Maguire, S.O. Shekhtman, S.H. Taylor, J. Catal. 276 (2010) 38.
[6] G.J. Hutchings, M.S. Hall, A.F. Carley, P. Landon, B.E. Solsona, C.J. Kiely, A. Herzing, M. Makkee, J.A. Moulijn, A. Overweg, J.C. Fierro-Gonzalez, J. Guzman, B.C. Gates, J. Catal. 242 (2006) 71.
[7] L. Li, A. Wang, B. Qiao, J. Lin, Y. Huang, X. Wang, T. Zhang, J. Catal. 299 (2013) 90.
[8] B.W. Wojciechowski, S.P. Asprey, Appl. Catal., A 190 (2000) 1.
[9] B.W. Wojciechowski, N.M. Rice, Experimental Methods in Kinetics Studies, Elsevier, Amsterdam, The Netherlands, 2003.
[10] I. Dobrosz-Gómez, I. Kocemba, J.M. Rynkowski, Appl. Catal., B 83 (2008) 240.
[11] I. Dobrosz-Gómez, I. Kocemba, J.M. Rynkowski, Appl. Catal., B 88 (2009) 83.
[12] T. Engel, G. Ertl, Adv. Catal. 28 (1979) 1.
[13] H. Provendier, C. Petit, J.-L. Schmitt, A. Kiennemann, C. Chaumont, J. Mater. Sci. 34 (1999) 4121.
[14] S. Ivanova, C. Petit, V. Pitchon, Appl. Catal., A 267 (2004) 191.
[15] I. Dobrosz, K. Jiratova, V. Pitchon, J.M. Rynkowski, J. Mol. Catal. A: Chem. 234 (2005) 187.
[16] I. Dobrosz-Gómez, I. Kocemba, J.M. Rynkowski, Pol. J. Environ. Stud. 15 (2006) 32.
[17] I. Kocemba, Przem. Chem. 3 (2003) 142.
[18] M.A. Vannice, Catal. Today 123 (2007) 18.
[19] S.C. Chapra, R.P. Canale, Numerical Methods for Engineers, sixth ed., McGraw Hill, New York, 2010.
[20] J. Guzman, S. Carrettin, A. Corma, J. Am. Chem. Soc. 127 (2005) 3286.
[21] Y.-M. Kang, B.-Z. Wan, Catal. Today 35 (1997) 379.
[22] A. Venugopal, M.S. Scurrell, Appl. Catal., A 258 (2004) 241.
[23] L. Ilieva, D. Andreeva, A. Andreev, Thermochim. Acta 292 (1997) 169.
[24] S. Scirè, M. Minicò, C. Crisafulli, C. Satriano, A. Pistone, Appl. Catal., B 40 (2003) 43.
[25] A.Q. Wang, Y.P. Hsieh, Y.F. Chen, C.Y. Mou, J. Catal. 237 (2006) 197.
[26] K. Qian, W. Huang, J. Fang, S. Lv, B. He, Z. Jiang, S. Wei, J. Catal. 255 (2008) 269.
[27] E. del Río, S.E. Collins, A. Aguirre, X. Chen, J.J. Delgado, J.J. Calvino, S. Bernal, J. Catal. 316 (2014) 210.